



## Free dendritic growth model incorporating interfacial nonisosolutal nature due to normal velocity variation

Shu LI<sup>1,2</sup>, Zhi-hui GU<sup>1</sup>, Da-yong LI<sup>2</sup>, Shuang-shuang WU<sup>3</sup>, Ming-hua CHEN<sup>1</sup>, Yu FENG<sup>1</sup>

1. College of Applied Science, Harbin University of Science and Technology, Harbin 150080, China;

2. College of Materials Science and Engineering, Harbin University of Science and Technology, Harbin 150080, China;

3. College of Civil Engineering and Architecture, Harbin University of Science and Technology, Harbin 150080, China

Received 22 December 2014; accepted 4 March 2015

**Abstract:** Considering both the effects of the interfacial normal velocity dependence of solute segregation and the local nonequilibrium solute diffusion, an extended free dendritic growth model was analyzed. Compared with the predictions from the dendritic model with isosolutal interface assumption, the transition from solutal dendrite to thermal dendrite moves to higher undercoolings, i.e., the region of undercoolings with solute controlled growth is extended. At high undercoolings, the transition from the mainly thermal-controlled growth to the purely thermal-controlled growth is not sharp as predicted by the isosolute model, but occurs in a range of undercooling, due to both the effects of the interfacial normal velocity dependence of solute segregation and the local nonequilibrium solute diffusion. Model test indicates that the present model can give a satisfactory agreement with the available experimental data for the Ni–0.7% B (mole fraction) alloy.

**Key words:** dendritic growth; interfacial nonisosolutal nature; modeling; binary alloy

### 1 Introduction

In past decades, numerous free dendritic growth models have been established, which include phase field models [1–3], models in the framework of microscopic solvability theory [4–6] and models based on Ivantsov approach [7–21]. Phase field models adopt an order parameter, i.e., phase-field variable  $\phi$  to describe the thermodynamic state of a local volume. This approach does not require tracking the solid–liquid interface and describes dynamical phenomena at the interface and in bulk phases through a single formalism. Microscopic solvability theory formulates dendritic growth problem as a single integro-differential equation and solves it without further hypotheses. The anisotropies of the interfacial energy and interfacial kinetics were taken into account, successfully. However, both of the phase field theory and microscopic solvability theory are very complicated, mathematically. It is not easy to be used for them, in practice. In contrast, the series of models based on Ivantsov approach received wide acceptance from

materials scientists, due to its relative simplicity as well as the ability to describe the solidification with dendritic morphology.

During steady-state free dendritic growth, the paraboloid of revolution is a good approximation for the dendrite tip shape [22]. Based on this assumption, IVANTSOV [7,8] first obtained the exact solutions of the classical Fick diffusion equations for solute and thermal diffusions in bulk liquids. Subsequently, a series of free dendritic growth models were proposed by adopting the Ivantsov results, such as the well-known BCT model [12], the models developed by GALENKO and DANILOV [13,14] and SOBOLEV [15,16]. In BCT model, the thermodynamic driving force, the kinetic undercooling and Aziz's solute trapping model [23] were introduced to describe high Peclet conditions. However, this model could only deal with the deviation from local equilibrium state at the solid–liquid interface. By introducing the local nonequilibrium diffusion model, the dendritic growth models developed by GALENKO and DANILOV [13,14] and SOBOLEV [15,16] could describe the local nonequilibrium state both at the

**Foundation item:** Project (51101046) supported by the National Natural Science Foundation of China; Project (E201446) supported by the Natural Science Foundation of Heilongjiang Province of China; Projects (2012M510985, 2014T70361) supported by China Postdoctoral Science Foundation; Project (LBH-Z12142) supported by the Heilongjiang Postdoctoral Fund, China

**Corresponding author:** Shu LI; Tel: +86-451-86390978; E-mail: [lishu@hrbust.edu.cn](mailto:lishu@hrbust.edu.cn)

DOI: 10.1016/S1003-6326(15)63971-1

interface and in bulk liquids. Recently, WANG et al [20] further extended the series of models to concentrated multi-component alloys. In all of these models, however, it is assumed that the interface is isothermal and isosolutal.

During steady-state growth, the normal velocity varies along the dendritic interface. This variation would lead to different solute partitioning along the interface and further lead to a nonisosolutal solid–liquid interface. It is also well known both from phase field and experiments, that the solute content in a dendritic structure has a typical appearance, i.e., high concentration along the stem and low concentration on both sides. Therefore, it is significant to analyze the effect of the interfacial normal velocity dependence of solute segregation on the dendritic solidification behavior. Recently, a generalized free dendritic growth model was developed by solving the classical Fick diffusion equation exactly under the boundary condition of nonisothermal and nonisosolutal interface [24]. However, the effect of local nonequilibrium solute diffusion in bulk liquid was not taken into account. In the present work, a relatively simple method was proposed to analyze both the effects of the interfacial normal velocity dependence of solute segregation and the local nonequilibrium solute diffusion. An experimental comparison with the available experimental data for the Ni–0.7%B (mole fraction) alloy was also made.

## 2 Model

In this section, two independent variables were introduced to describe the dendritic morphology during steady state solidification. Based on this interfacial morphology, the solute trapping model recently developed by LI and SOBOLEV [25] was outlined. Then taking into account the interfacial driving force, an interfacial response function was proposed, approximately. From this interfacial response function, the tip radius of curvature was derived. Finally, an extended free dendritic growth model was obtained for binary alloys, which could deal with both the interfacial normal velocity dependence of solute segregation and the local nonequilibrium solute diffusion.

### 2.1 Extended solute trapping model

During steady-state solidification, the dendritic morphology could be approximated by a paraboloid of revolution [22]. For describing the interfacial morphology with the paraboloid of revolution uniquely, it is required mathematically to introduce the radius of curvature ( $R$ ) at the dendrite tip. This parameter has been widely adopted in previous dendritic models [9–21]. In the present work, taking into account the interfacial

normal velocity dependence of solute partitioning, it is not enough to only adopt the parameter  $R$ . Here, an angle ( $\theta$ ) is introduced. The normal direction at an interface element makes the angle  $\theta$  with respect to the growth axis. For steady-state growth at a given interface migration velocity  $V$  (i.e., tip velocity), there is a critical value of the angle  $\theta$ . This critical angle  $\theta$ , i.e., the maximum angle, is marked by  $\theta_{\max}$ . For  $\theta \geq \theta_{\max}$ , the solid–liquid interface becomes unstable and the secondary dendrite arm and necking phenomenon may appear. The present model focuses on the range of  $0 \leq \theta \leq \theta_{\max}$ , which corresponds to the shape preserving part of the dendritic interface. Therefore, considering the interfacial normal velocity dependence of solute segregation, one should use both the parameter  $R$  and the angle  $\theta_{\max}$  to describe the steady-state shape and the boundary.

Along the dendritic interface from the tip ( $\theta=0$ ) to the root ( $\theta=\theta_{\max}$ ), the normal velocity  $V_n$  decreases, which could be described by  $V_n(\theta)=V\cos\theta$  due to the shape preserving condition. The normal velocity  $V_n(\theta)$  can be regarded as the effective velocity which controls the solute redistribution at the interface element marked by angle  $\theta$ . Introducing this dependence of  $V_n$  on  $\theta$  into the solute trapping model proposed by SOBOLEV [15,16], the solute partition coefficient  $K$  could be further described as [25]

$$K(V, \theta) = \begin{cases} \frac{K_E(1-V^2 \cos^2 \theta / V_D^2) + V \cos \theta / V_{DI}}{(1-V^2 \cos^2 \theta / V_D^2) + V \cos \theta / V_{DI}}, & V \cos \theta < V_D \\ 1, & V \cos \theta \geq V_D \end{cases} \quad (1)$$

where  $K_E$  is the equilibrium partition coefficient,  $V_{DI}$  is the interface diffusive speed and  $V_D$  is the bulk liquid diffusive speed.

In order to analyze the effect of the interfacial normal velocity dependence of solute segregation on the dendritic solidification behavior, it is useful to calculate the average of partition coefficient  $\bar{K}(V)$  from the tip to the root of the dendrite. For the interface approximated by a paraboloid of revolution,  $\bar{K}(V)$  could be given as follows [25]:

$$\bar{K}(V) = \begin{cases} \frac{3 \int_0^{\theta_{\max}} K(V, \theta) \exp(3\theta) d\theta}{\exp(3\theta_{\max}) - 1}, & V \cos \theta_{\max} < V_D \\ 1, & V \cos \theta_{\max} \geq V_D \end{cases} \quad (2)$$

### 2.2 Interfacial response function

In previous models, the driving force on solidification, i.e., the effective driving free energy  $\Delta G_{\text{EFF}}$  was calculated with the values for liquid solute

concentration ( $C_L^*$ ) and solid solute concentration ( $C_S^*$ ) at the dendrite tip ( $\theta=0$ ), due to the isosolutal interface assumption [12–21]. In the present work, taking into account the dependence of  $K(V, \theta)$  on  $\theta$ , the interfacial composition is not constant. Therefore, as an approximation, the effective driving free energy  $\Delta G_{\text{EFF}}$  could be evaluated based on the average values of the interfacial solute concentration  $\overline{C_L^*}$  and  $\overline{C_S^*}$ . Following the Galenko's analysis based on the extended irreversible thermodynamics [26], the effective driving free energy  $\Delta G_{\text{EFF}}$  can be given as

$$\Delta G_{\text{EFF}} = (1 - \overline{C_L^*})\Delta\mu_1 + \overline{C_L^*}\Delta\mu_2 + (\overline{C_L^*} - \overline{C_S^*})(1 - \overline{K})R_g T_1 V / V_D, \quad V \cos \theta_{\max} < V_D \quad (3)$$

$$\Delta G_{\text{EFF}} = (1 - \overline{C_S^*})\Delta\mu_1 + \overline{C_S^*}\Delta\mu_2, \quad V \cos \theta_{\max} \geq V_D \quad (4)$$

where  $\Delta\mu_1$  and  $\Delta\mu_2$  are the chemical potential changes upon solidification for solvent and solute, respectively;  $R_g$  is the gas constant, and  $T_1$  is the interfacial temperature, which is assumed to be constant along the interface. For sufficiently dilute alloys, the Henry's law is valid. Thus, based on the analysis of BAKER and CAHN [27],  $\Delta\mu_1$  and  $\Delta\mu_2$  could be approximated by

$$\Delta\mu_1 = R_g T_1 \ln \frac{(1 - \overline{C_S^*})(1 - C_L^{\text{eq}})}{(1 - C_L^*) (1 - C_S^{\text{eq}})} = R_g T_1 (\overline{C_L^*} - \overline{C_S^*} + C_S^{\text{eq}} - C_L^{\text{eq}}) \quad (5)$$

$$\Delta\mu_2 = R_g T_1 \ln \left( \frac{\overline{K}}{K_E} \right) \quad (6)$$

where  $C_L^{\text{eq}}$  and  $C_S^{\text{eq}}$  are the equilibrium solute concentrations at the interface, for the temperature  $T_1 + \Delta T_R$ . Here, the curvature correction is considered and  $\Delta T_R$  is the curvature undercooling defined by  $2\Gamma/R$  ( $\Gamma$  is the Gibbs–Thompson coefficient,  $R$  is the radius of curvature).

For sufficiently dilute alloys, the linear liquidus and solidus line approximation is reasonable. Combining this linear approximation and Baker and Chan's approximation [27], Eqs. (5) and (6), with Turnbull's collision-limited growth law  $\Delta G_{\text{EFF}}/(R_g T_1) + V/V_0 = 0$  [28], one can obtain the interfacial response function as follows:

$$T_1 = T_M + m(V)\overline{C_L^*} - V/\mu_0 - 2\Gamma/R \quad (7)$$

where  $T_M$  is the melting point of pure solvent,  $\mu_0$  is the kinetic coefficient defined by  $V_0(K_E - 1)m_E$ ,  $V_0$  is the maximum crystallization velocity,  $m_E$  is the equilibrium liquidus slope and  $m(V)$  is the kinetic liquidus slope given by

$$m(V) = \frac{m_E}{1 - K_E} \left[ 1 - \overline{K} + \ln \left( \frac{\overline{K}}{K_E} \right) + (1 - \overline{K})^2 \frac{V}{V_D} \right], \quad V \cos \theta_{\max} < V_D \quad (8)$$

$$m(V) = \frac{m_E \ln K_E}{K_E - 1}, \quad V \cos \theta_{\max} \geq V_D \quad (9)$$

In the present model, taking into account the interfacial normal velocity dependence of solute partitioning, the solid–liquid interface is nonisosolutal. Along the dendritic side from the tip to the root, the solute partition coefficient  $K(V, \theta)$  decreases and the liquid solute concentration  $C_L^*(\theta)$  increases. Based on the Ivantsov treatment for solute diffusion [7,8], the average solute concentration along the interface  $\overline{C_L^*}$  could be approximated by

$$\overline{C_L^*} = \frac{C_0}{1 - [1 - \overline{K(V)}] \text{Iv}(P_c)}, \quad V \cos \theta_{\max} < V_D \quad (10)$$

$$\overline{C_L^*} = C_0, \quad V \cos \theta_{\max} \geq V_D \quad (11)$$

where  $C_0$  is the nominal composition of alloys,  $P_c = RV/(2D_L)$  is the solutal Peclet number,  $D_L$  is the solute diffusion coefficient in liquid and Iv is the Ivantsov function [7,8]. In addition, based on the Ivantsov approach for thermal diffusion, the interfacial temperature  $T_1$  in the interfacial response function, Eq. (7), is given as follows, with the isothermal interface approximation,

$$T_1 = \frac{\Delta H_f}{c_p} \text{Iv}(P_t) + T_\infty \quad (12)$$

where  $\Delta H_f$  is the latent heat of fusion,  $c_p$  is the specific heat capacity of liquid alloy,  $P_t = RV/(2a_L)$  is the thermal Peclet number,  $a_L$  is the thermal diffusivity in liquid and  $T_\infty$  is the temperature of undercooled melt far from the tip. Combining Eqs. (7) and (12), one could describe the bath undercooling  $\Delta T$  as

$$\Delta T = \left[ m_E C_0 - m(V)\overline{C_L^*} \right] + \frac{V}{\mu_0} + \frac{2\Gamma}{R} + \frac{\Delta H_f}{c_p} \text{Iv}(P_t) \quad (13)$$

It should be noted that the Ivantsov results for the description of  $C_L^*(\theta)$  is adopted in the present treatment. Strictly speaking, the Ivantsov results are only suitable for the isosolutal interface condition. The present model provides an approximated method to analyze the effect of the interfacial normal velocity dependence of solute segregation. For more exact solution, the model given in Ref. [24] should be further extended.

### 2.3 Tip radius of curvature

Based on the marginal stability theory [29–34], adopting the planar interface response function (Eq. (7)), in which the curvature undercooling  $2\Gamma/R$  is removed, and combined with Langer and Muller–Krumhhaar approximation [35], one could describe the radius of curvature  $R$  as

$$R = \frac{\Gamma / \sigma^*}{\frac{P_i \Delta H_f}{c_p} \xi_t + \frac{2m(V)[(\overline{K}(V)-1)C_L^* P_c^* \xi_c}{1 - (V \cos \theta_{\max})^2 / V_D^2} \xi_c}, \quad V \cos \theta_{\max} < V_D \quad (14)$$

$$R = \frac{\Gamma / \sigma^*}{\frac{P_i \Delta H_f}{c_p} \xi_t}, \quad V \cos \theta_{\max} \geq V_D \quad (15)$$

where  $\sigma^*$  is the stability constant ( $\sigma^* \approx 1/4\pi^2$ ) and the parameters  $\xi_t$  and  $\xi_c$  are defined as follows:

$$\xi_t = 1 - \frac{1}{\sqrt{1 + (\sigma^* P_i^2)^{-1}}} \quad (16)$$

$$\xi_c = 1 - \frac{2\overline{K}}{\sqrt{1 + [1 - (V \cos \theta_{\max})^2 / V_D^2] / (\sigma^* P_c^2) + 2\overline{K} - 1}}, \quad V \cos \theta_{\max} < V_D \quad (17)$$

$$\xi_c = 0, \quad V \cos \theta_{\max} \geq V_D \quad (18)$$

Integrating Eq. (2) and Eqs. (7)–(18) gives the dendritic solidification behavior uniquely, such as the interfacial migration velocity  $V$ , the dendritic tip radius  $R$ , the profiles of the solute partition coefficient  $K(V, \theta)$  and the liquid solute concentration  $C_L^*(\theta)$  along the interface as well as the average partition coefficient  $\overline{K}(V)$ .

### 3 Discussion and comparison with experiment

Taking into account the interfacial normal velocity dependence of solute partitioning, the present model could describe the nonisolutal nature of the solid–liquid interface. For making a comparison between the present model and the corresponding model with the assumption of isolutal interface, i.e. Gelenko and Danilov model [13,14], Ni–0.7%B (mole fraction) alloy was adopted in model computations. The parameters used are listed in Table 1. The calculated results are shown in Figs. 1–3, including the interfacial migration velocity  $V$ , the dendritic tip radius  $R$  and the partition coefficient  $K$  as functions of the bath undercooling  $\Delta T$ .

In Fig. 1, four undercoolings,  $\Delta T_1$ ,  $\Delta T_2$ ,  $\Delta T_3$  and  $\Delta T_4$ , are defined for the present model, which determine five ranges of bath undercooling  $\Delta T$ .  $\Delta T_1$  is the critical undercooling, at which the velocity  $V$  coincides with the critical velocity of absolute solute stability  $V_c^*$  [19]. At  $\Delta T < \Delta T_1$ , the dendritic growth is mainly controlled by solute diffusion, and at  $\Delta T = \Delta T_1$ , the transition from mainly solute controlled growth to mainly thermal controlled growth occurs. As shown in Fig. 1, the range 2 of  $\Delta T$  is the transition region, and at  $\Delta T = \Delta T_2$ , this transition completes.  $\Delta T_2$  is defined by the critical

**Table 1** Thermodynamic parameters for Ni–0.7%B (mole fraction) alloy used in model computations [13]

Parameter	Value
Mole fraction of boron /%	0.7
Melting point of pure Ni, $T_M$ /K	1726
Specific heat of fusion, $\Delta H_f$ /(J·mol <sup>-1</sup> )	$1.72 \times 10^4$
Specific heat capacity, $c_p$ /(J·mol <sup>-1</sup> ·K <sup>-1</sup> )	36.39
Capillarity constant, $\Gamma$ /(K·m)	$3.42 \times 10^{-7}$
Diffusion coefficient, $D_L$ /(m <sup>2</sup> ·s <sup>-1</sup> )	$5.5 \times 10^{-9}$
Thermal diffusivity, $a_L$ /(m <sup>2</sup> ·s <sup>-1</sup> )	$8.5 \times 10^{-6}$
Interfacial diffusion speed, $V_{DI}$ /(m·s <sup>-1</sup> )	16.2
Diffusion speed in bulk liquid, $V_D$ /(m·s <sup>-1</sup> )	18.9
Liquidus slope, $m_E$ /(K·% <sup>-1</sup> )	-14.3
Partition coefficient, $k_E$	0.0155
Kinetic coefficient, $\mu_0$ /(m·s <sup>-1</sup> ·K <sup>-1</sup> )	0.25

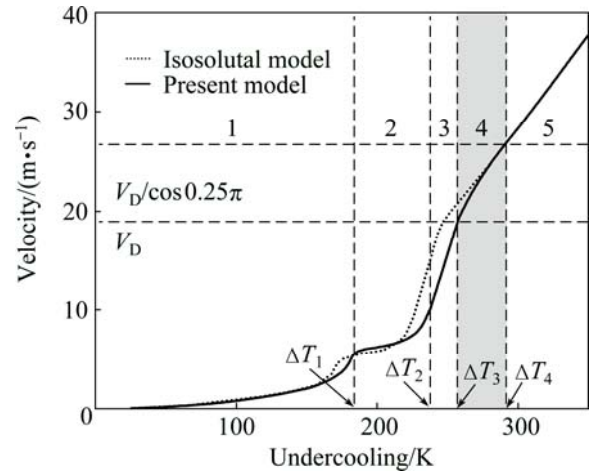


**Fig. 1** Interfacial migration velocity  $V$  vs bath undercooling  $\Delta T$  predicted by isolutal model [13,14] and present model ( $\theta_{\max} = 0.25\pi$ ) for Ni–0.7%B alloy (mole fraction)

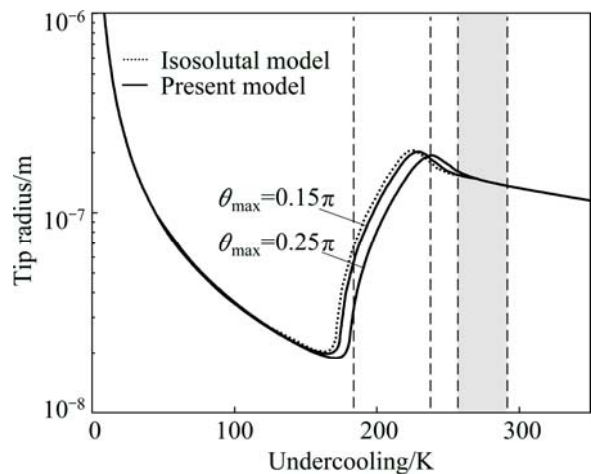


**Fig. 2** Tip radius of curvature vs bath undercooling predicted by isolutal model [13,14] and present model for Ni–0.7%B alloy (For the present model two different values of  $\theta_{\max}$  were adopted)

undercooling, at which the tip radius  $R$  attains its extreme point. When  $\Delta T$  is larger than  $\Delta T_2$ , the tip radius  $R$  decreases monotonically with increasing  $\Delta T$  (Fig. 2).  $\Delta T_3$  is the critical undercooling, at which the interfacial velocity  $V$  equals the bulk liquid diffusive velocity  $V_D$ . And  $\Delta T_4$  corresponds to a bath undercooling, at which the normal velocity  $V_n=V_D$  at the dendrite root ( $\theta=\theta_{\max}$ ), i.e., the dendritic growth velocity  $V=V_D/\cos\theta_{\max}$ . It is noted that  $\theta_{\max}=0.25\pi$  was used in Fig. 1 as an example.

Under the condition that the interface velocity  $V$  is of the order or larger than the solute diffusion velocity  $V_D$ , the solute diffusion is in local nonequilibrium. Taking into account the nonequilibrium nature of diffusion, the isosolutal model predicts that at  $V \geq V_D$ , complete solute trapping occurs (Fig. 3) and the transition at  $V=V_D$  is sharp (Fig. 1). This indicates that the transition from mainly thermal controlled growth to purely thermal controlled growth is sharp. For the isosolutal model, these predictions are based on the assumption that the dendritic interface including the tip is isosolutal. In reality, however, it is obvious that during steady-state solidification, the normal velocity  $V_n$  is not constant along the dendritic interface. For solute redistribution at the solid–liquid interface, the normal velocity  $V_n$  is the decisive factor. Therefore, the solid–liquid interface is nonisosolutal. The present model provides an approach to deal with the effect of the interfacial normal velocity variation. As described by Fig. 3, at  $V=V_D$ , i.e.,  $\Delta T=\Delta T_3$ , the complete solute trapping ( $K=1$ ) only occurs at the dendrite tip due to  $V_n < V_D$  at the other parts of the dendritic interface. With increasing  $\Delta T$ , the interface velocity  $V$  increases and  $K=1$

occurs at the interface with more elements. When  $V=V_D/\cos\theta_{\max}$  ( $\Delta T=\Delta T_4$ ), for the root of dendrite  $K=1$  and thus the complete solute trapping achieves at the whole interface ( $0 \leq \theta \leq \theta_{\max}$ ). Therefore, considering the interfacial normal velocity dependence of solute partitioning, the transition to partitionless solidification is not sharp, but occurs in a range of  $\Delta T$ . This transition is shown by the grey region in Figs. 1–3, i.e., the range 4 of  $\Delta T$ . At  $\Delta T \geq \Delta T_4$ , purely thermal controlled growth occurs. Under this condition, the solidification behavior is the same as that for pure metals.

Another effect of the interfacial normal velocity dependence of solute partitioning is the transition region of undercooling from mainly solute controlled growth to mainly thermal controlled growth (the range 2 of  $\Delta T$ ). As indicated by Figs. 1–3, the effect of the interfacial normal velocity dependence of solute partitioning leads to that the transition region moves to higher undercooling, i.e., the region with solute controlled growth is extended. This is because that the average partition coefficient is considered in the present model to deal with the effect of the nonisosolutal interface. Along the interface from the tip to the root, the partition coefficient  $K(V, \theta)$  decreases as described by Eq. (1), since the normal velocity  $V_n$  decreases. Thus, the average partition coefficient is less than the partition coefficient at the dendrite tip (Fig. 3). This implies that the degree of average solute segregation is larger than that at the tip. Therefore, the undercooling region with solute-controlled growth is extended under the nonisosolutal interface condition. In addition, with increasing the interfacial region with steady-state growth marked by  $\theta_{\max}$ , the solutal dendrite region of undercooling is further extended (Figs. 1–3) and thus the effect of the interfacial normal velocity dependence of solute partitioning is more significant.

In order to further validate the present model, a comparison with the available experimental data for Ni–0.7%B alloy was made. The related values of the parameters used in the model computation are given in Table 1. The insert in Fig. 3 shows the data points from the electromagnetic levitation experiment [35] and the predicted dendritic growth velocity as a function of the bath undercooling  $\Delta T$  for the present model. It is noted that  $\theta_{\max}=0.15\pi$  was adopted as a fitting parameter to obtain a better description for the experiment results. As can be seen clearly, the present model gives an agreement with the experimental data.

As indicated by Fig. 1, at  $V=V_D/\cos\theta_{\max}$  ( $\Delta T=\Delta T_4$ ), the complete solute trapping occurs at the whole interface  $0 \leq \theta \leq \theta_{\max}$  with steady-state growth. And the transition to complete partitionless solidification is not sharp, but occurs in the range 4 of  $\Delta T$  marked by the grey region. Thus, with increasing the value for  $\theta_{\max}$ , the

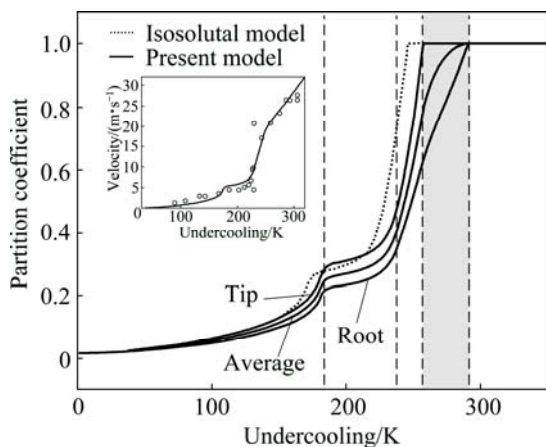


**Fig. 3** Partition coefficient as functions of bath undercooling predicted by isosolutal model [13,14] and present model for Ni–0.7%B alloy (For the present model,  $\theta_{\max}=0.25\pi$  was adopted as an example. The insert shows the relationship between the interfacial migration velocity and the bath undercooling. The solid line is the result predicted by the present model with  $\theta_{\max}=0.15\pi$  and the open circles denote the experimental data for Ni–0.7%B alloy [36])

transition region, i.e., the range 4 of  $\Delta T$  is extended and the effect of the interfacial normal velocity dependence of solute partitioning is more significant. From the present experimental comparison,  $\theta_{\max}$  with the value of  $0.15\pi$  is obtained as a fitting parameter. It is small and the corresponding transition region is also narrow with the value of 10 K ( $\Delta T_4 - \Delta T_3$ ). This can also be found from Fig. 2, in which the difference is not remarkable between the predictions from the isosolutal model and the present model with  $\theta_{\max} = 0.15\pi$  for the tip radius. Therefore, it implied that the effect of the interfacial normal velocity dependence of solute partitioning is relatively small for the Ni–0.7%B alloy. Furthermore, the present model can also describe the transition of growth mode from the power law to linear growth due to the narrow transition region.

It should be stressed that the critical angle  $\theta_{\max}$  was introduced into the present model to characterize the shape preserving part of dendritic interface during steady-state growth and the angle  $\theta_{\max}$  was used as a fitting parameter in the present work. Strictly speaking, at different interfacial migration velocities  $V$ , the shape of interface is also different, and thus the values of  $R$  and  $\theta_{\max}$  are variable. The relationship between  $V$  and  $R$  could be described by marginal stability theory (see Eqs. (14) and (15)). Also, there should be another relationship between  $V(R)$  and  $\theta_{\max}$ . For a very large tip radius  $R$ , i.e., when the solid–liquid interface tends to planar one,  $\theta_{\max}$  would be very small. In contrast,  $\theta_{\max}$  could even reach  $\pi/2$  if  $R$  is very small. This problem should be further studied.

## 4 Conclusions

1) A free dendritic growth model was proposed for binary alloys, which could deal with both the interfacial normal velocity dependence of solute partitioning and the local nonequilibrium solute diffusion. Numerical test indicates that the solutal dendrite region of undercooling is extended due to the effect of the interfacial normal velocity dependence of solute partitioning for the present model, compared with the isosolutal model.

2) At high undercoolings, when the solidification velocity is of the order or larger than the solute diffusive velocity, the transition to diffusionless solidification is not sharp as predicted by the isosolute model, but occurs in a range of undercoolings. This is because that the present model considered both the effects of the interfacial normal velocity dependence of solute partitioning and the local nonequilibrium solute diffusion.

3) With increasing the interfacial region with steady-state growth, the effect of the interfacial normal velocity dependence of solute segregation is more

significant. Furthermore, it is also shown that the present model provides a satisfactory agreement with the available experimental data.

## References

- [1] BOETTINGER W J, CORIELL S R, GREER A L, KARMA A, KURZ W, RAPPAZ M, TRIVEDI R. Solidification microstructures: Recent developments, future directions [J]. *Acta Materialia*, 2000, 48: 43–70.
- [2] ECHEBARRIA B, FOLCH R, KARMA A, PLAPP M. Quantitative phase field model of alloy solidification [J]. *Physical Review E*, 2004, 70: 061604.
- [3] GALENKO P K, REUTZEL S, HERLACH D M, DANILOV D A, NESTLER B. Modelling of dendritic solidification in undercooled dilute Ni–Zr melts [J]. *Acta Materialia*, 2007, 55: 6834–6842.
- [4] KESSLER D, KOPLIK J, LEVINE H. Pattern selection in fingered growth phenomena [J]. *Advances in Physics*, 1988, 37: 255–339.
- [5] BARBIERI A, LANGER J S. Predictions of dendritic growth rates in the linearized solvability theory [J]. *Physical Review A*, 1989, 39: 5314–5325.
- [6] BRENER E A, MEL'NIKOV V I. Pattern selection in two-dimensional dendritic growth [J]. *Advances in Physics*, 1991, 40: 53–97.
- [7] IVANTSOV G P. Temperature field around spherical, cylindrical, and needle-shaped crystals which grow in supercooled melts [J]. *Dokl Akad Nauk SSSR*, 1947, 58: 567–569. (in Russian)
- [8] IVANTSOV G P. On the growth of a spherical or a needlelike crystal of a binary alloy [J]. *Dokl Akad Nauk SSSR*, 1952, 83: 573–576.
- [9] LIPTON J, GLICKSMAN M E, KURZ W. Free dendritic growth [J]. *Materials Science and Engineering*, 1984, 65: 45–55.
- [10] LIPTON J, KURZ W, TRIVEDI R. Effect of growth rate dependent partition coefficient on the dendritic growth in undercooled melts [J]. *Acta Metallurgica*, 1987, 35: 957–970.
- [11] TRIVEDI R, LIPTON J, KURZ W. Effect of growth rate dependent partition coefficient on the dendritic growth in undercooled melts [J]. *Acta Metallurgica*, 1987, 35: 965–970.
- [12] BOETTINGER W J, CORIELL S R, TRIVEDI R. Rapid solidification processing: Principles and technologies IV [M]. Baton Rouge, LA: Claitor's, 1988: 13–24.
- [13] GALENKO P K, DANILOV D A. Local nonequilibrium effect on rapid dendritic growth in a binary alloy melt [J]. *Physics Letters A*, 1997, 235: 271–280.
- [14] GALENKO P K, DANILOV D A. Model for free dendritic alloy growth under interfacial and bulk phase nonequilibrium conditions [J]. *Journal of Crystal Growth*, 1999, 197: 992–1002.
- [15] SOBOLEV S L. Rapid solidification under local nonequilibrium conditions [J]. *Physical Review E*, 1997, 55: 6845–6854.
- [16] SOBOLEV S L. An analytical model for local-nonequilibrium solute trapping during rapid solidification [J]. *Transactions of Nonferrous Metals Society of China*, 2012, 22(11): 2749–2755.
- [17] DIVENUTI A G, ANDO T. A free dendritic growth model accommodating curved phase boundaries and high Peclet number conditions [J]. *Metallurgical and Materials Transactions A*, 1998, 29: 3047–3056.
- [18] ÖNEL S, ANDO T. Comparison and extension of free dendritic growth models through application to a Ag-15 mass pct Cu alloy [J]. *Metallurgical and Materials Transactions A*, 2008, 39: 2449–2458.
- [19] WANG H F, LIU F, CHEN Z, YANG G C, ZHOU Y H. Analysis of non-equilibrium dendrite growth in a bulk undercooled alloy melt: Model and application [J]. *Acta Materialia*, 2007, 55: 497–506.
- [20] WANG K, WANG H F, LIU F, ZHAI H M. Modeling dendrite growth in undercooled concentrated multi-component alloys [J]. *Acta*

- Materialia, 2013, 61: 4254–4265.
- [21] LI S, ZHANG J, WU P. Analysis for free dendritic growth model applicable to monodilute alloys [J]. Metallurgical and Materials Transactions A, 2012, 43: 3748–3754.
- [22] TRIVEDI R, KURZ W. Dendritic growth [J]. International Materials Reviews, 1994, 39: 49–74.
- [23] AZIZ M J. Model for solute redistribution during rapid solidification [J]. Journal of Applied Physics, 1982, 53: 1158–1168.
- [24] LI S, LI D, LIU S, GU Z, LIU W, HUANG J. An extended free dendritic growth model incorporating the nonisothermal and nonisolutal nature of the solid–liquid interface [J]. Acta Materialia, 2015, 83: 310–317.
- [25] LI S, SOBOLEV S L. Local nonequilibrium solute trapping model for non-planar interface [J]. Journal of Crystal Growth, 2013, 380: 68–71.
- [26] GALENKO P K. Extended thermodynamical analysis of a motion of the solid-liquid interface in a rapidly solidifying alloy [J]. Physical Review B, 2002, 65: 144103.
- [27] BAKER J C, CAHN J W. Solidification [M]. Ohio: American Society Metals, Metals Park, 1970: 23–58.
- [28] TURNBULL D. On the relation between crystallization rate and liquid structure [J]. The Journal of Physical and Chemistry, 1962, 66: 609–613.
- [29] MULLINS W W, SEKERKA R F. Stability of a planar interface during solidification of a dilute binary alloy [J]. Journal of Applied Physics, 1964, 35: 444–451.
- [30] TRIVEDI R, KURZ W. Morphological stability of a planar interface under rapid solidification conditions [J]. Acta Metallurgica, 1986, 34: 1663–1670.
- [31] GALENKO P K, DANILOV D A. Linear morphological stability analysis of the solid-liquid interface in rapid solidification of a binary system [J]. Physical Review E, 2004, 69: 051608.
- [32] WANG H F, LIU F, YANG W, CHEN Z, YANG G C, ZHOU Y H. An extended morphological stability model for a planar interface incorporating the effect of nonlinear liquidus and solidus [J]. Acta Materialia, 2008, 56: 2592–2601.
- [33] WANG K, WANG H F, LIU F, ZHAI H M. Morphological stability analysis for planar interface during rapidly directional solidification of concentrated multi-component alloys [J]. Acta Materialia, 2013, 67: 220–231.
- [34] LI S, ZHANG J, WU P. Numerical test of generalized marginal stability theory for a planar interface during directional solidification [J]. Scripta Materialia, 2009, 61: 485–488.
- [35] LANGER S, MULLER-KRUMBHAAR H. Theory of dendritic growth—I. Elements of a stability analysis [J]. Acta Metallurgica, 1978, 26: 1681–1687.
- [36] ECKLER K, COCHRANE R F, HERLACH D M, FEUERBACHER B, JURISCH M. Evidence for a transition from diffusion-controlled to thermally controlled solidification in metallic alloys [J]. Physical Review B, 1992, 45: 5019–5022.

## 考虑界面法向速度变化所导致的 界面非等溶质特性的自由枝晶生长模型

李 述<sup>1,2</sup>, 谷志慧<sup>1</sup>, 李大勇<sup>2</sup>, 吴双双<sup>3</sup>, 陈明华<sup>1</sup>, 冯 宇<sup>1</sup>

1. 哈尔滨理工大学 应用科学学院, 哈尔滨 150080;

2. 哈尔滨理工大学 材料科学与工程学院, 哈尔滨 150080;

3. 哈尔滨理工大学 建筑工程学院, 哈尔滨 150080

**摘 要:** 在同时考虑溶质偏析的界面法向速度依赖性与局域非平衡溶质扩散的情况下, 建立一个扩展的自由枝晶生长模型。与假设等溶质界面的枝晶生长模型的预测相比, 从溶质枝晶到热枝晶的转变发生在更高的过冷度, 即溶质控制生长发生在更宽的过冷度区域。在高过冷度区域, 从热控制生长模式到纯热控制生长模式的转变没有等溶质模型所预测的急剧, 而是发生在一定范围的过冷度区域。这是由于溶质偏析的界面法向速度依赖性与局域非平衡溶质扩散这两个因素共同作用的结果。模型测试表明: 本模型能够对现有 Ni–0.7%B(摩尔分数)合金的实验数据给出满意的描述。

**关键词:** 枝晶生长; 界面非等溶质特性; 建模; 二元合金

(Edited by Xiang-qun LI)